ACS OMEGA

Open Access

http://pubs.acs.org/journal/acsodf

Article

Mesophase Behavior of Molecules Containing Three Benzene Rings Connected via Imines and Ester Linkages

Fowzia S. Alamro, Hoda A. Ahmed,* Nuha Salamah Alharbi, Nada S. Al-Kadhi, Omaima A. Alhaddadd, Magdi M. Naoum, and Mohamed A. El-Atawy*

Cite This: *ACS Omega* 2024, 9, 31601−31610

Read Online

ACCESS | Metrics & More | Article Recommendations | Supporting Information

ABSTRACT: Ten new compounds based on the methineazo-azomethine (CH═N−N═CH) and ester linking groups were prepared and investigated for their mesophase behavior and optical stability, and liquid crystals of 4-substituted phenyl methineazo-azomethine phenyl 4-alkoxybenzoates, In_{a-e}, were investigated. An alkoxy group with a length between 8 and 12 carbons is attached to the phenyl eater wing, while the other terminal ring is substituted in its 4-position with one of the polar NO_2, F, Cl, CH_3O, and $N(CH_3)_2$ groups. The molecular structures of the newly prepared compounds were verified by using ^1H NMR, ^{13}C NMR, and elemental analysis. Differential scanning calorimetry and polarized optical microscopy were applied to investigate their mesophase behavior. All members of the prepared homologous series showed excellent thermal mesomorphic stability over wide temperature ranges. The geometrical and thermal properties of the investigated compounds were verified via density functional theory (DFT). The theoretical results revealed that all of the compounds are almost planar. Finally, the experimentally established values of the mesophase data were correlated with the predicted quantum chemical characteristics evaluated by DFT.

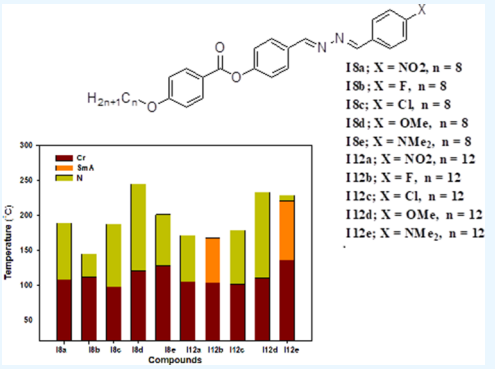

1. INTRODUCTION

Liquid crystals are materials that exist in a state of matter that exhibits the properties of both liquids and crystals. They have attracted considerable attention due to their unique optical, electrical, and mechanical properties. Liquid crystals have numerous applications in liquid crystal displays (LCDs), optical sensors, telecommunication devices, and many others.[1−7] Bis-Schiff base is an important linker group that links two different types of aromatic rings together, producing a linear molecular structure.[8] Thus, it can be used in mesogenic molecules, particularly in liquid crystals. One of the most significant properties of the bis-Schiff base linker group is its ability to form strong intermolecular interactions.[8] This property is crucial for the formation of ordered structures in liquid crystals, where intermolecular interactions between mesogens are important for maintaining the liquid crystal phase. Moreover, the aromatic rings of the bis-Schiff base can also participate in $\pi-\pi$ stacking interactions, which further enhance the ordering ability of the mesogen.[8] Another criterion of bis-Schiff base as a linker group is its ability to tune the physical properties of the liquid crystal by varying the nature of the substituents attached to the aromatic rings.[8] For example, the inclusion of electron-donating or -withdrawing moieties can modify the strength of the intermolecular interactions and tune the mesogen's melting point, viscosity, and birefringence. Furthermore, bis-Schiff bases are known for their relative mesomorphic stability and robust nature, which are important for the fabrication of LCDs.[9] Due to their high mesomorphic stability, these Schiff base-based mesogens would improve their temperature regions according to their packing behavior, which makes them ideal for various applications in modern technology.[10]

Many different kinds of liquid crystal compounds have been synthesized using Schiff bases as a connecting group.[11−15] The primary forms of connectors within the cores are functional groups with dipole associations, such as ester or amido groups.[16,17] The production, kind, mesomorphic stability, and temperature range of the mesomorphic material have all been observed to be significantly influenced by the central bridges and the end groups.[18−23] Numerous thermotropic liquid crystals of the Schiff base type and low molar masses have been created and studied.[24−26] Additionally, it has been noted that several mesogenic homologous series include two central connections, one of which may be an ester and the other an azomethine.[27,28] Sometimes, traditional methods of new material design and development may not yield satisfactory results. Therefore,

Received: February 18, 2024
Revised: June 21, 2024
Accepted: July 2, 2024
Published: July 12, 2024

finding an alternative route becomes an urgent need. Due to their crucial significance in the discovery of novel materials, the reduction of the high costs and lengthy time requirements of materials research, and the quick transformation of new materials into products, theoretical calculations have recently become a crucial component of material design.[29−32]

To make molecular synthesis and device manufacturing easier, it is crucial to have an extensive understanding of the structures and properties of newly created materials.[33−35] Several computational approaches have been used in facilitating the designing of layered and inorganic crystals,[36] two-dimensional compounds for energy-related materials[29,33,36] functional organic materials,[29,35,37] and polymeric materials.[29,38] In addition, the combination of theoretical computation and experiment is widely used to obtain an in-depth understanding of the synthesized material structure and properties and generate directional design strategies for experiments.[39]

The influence of terminal flexible chain lengths on the mesophase behavior using novel homologous series carrying the bis-azomethine central linkage, ((1*E*,10*E*)-hydrazine-1,2-diylidenebis(methanylylidene)) bis(4,1-phenylene) dialkanoate, has been reported.[8] Herein, the current work aims to prepare (*E*)-4-((4-(trifluoromethyl)phenyl)diazenyl)phenyl 4-alkoxybenzoate (**I***n*$_x$, Figure 1) to investigate the correlation between the molecular structure and property of mesomorphic compounds with bis-Schiff base central linkages.

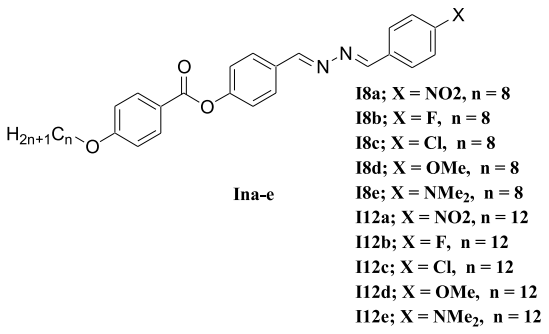

Figure 1. Structure of 4-substituted phenyl methine/azo-azo/methine phenyl 4-alkoxybenzoates **I***n*$_{a-e}$.

2. RESULTS AND DISCUSSION

2.1. Liquid Crystalline Characteristics of Series In$_x$.

Table 1 and Figure 2 provide the differential scanning calorimetry (DSC) measurements of the transition temperatures and associated enthalpies and entropies for all synthetic series **I***n*$_x$. All of the derivatives were found to be mesomorphically stable, as demonstrated by the consistency of the heating and cooling DSC curves. The DSC heating and cooling traces for compound **I12**$_e$ are shown in Figure 3. The transition temperatures and enthalpy values are calculated using the results of the second heating scan.

Following heating, the example compound, **I12**$_e$, in Figure 3's DSC thermogram was found to exhibit three endotherms that are assigned to the crystal−smectic, smectic−nematic, and nematic−isotropic liquid transitions. The compound exclusively exhibits the nematic and smectic phases during the heating and cooling cycles; however, their transitions shifted slightly at lower temperatures in the heating cycle. Mesophase textures were confirmed by polarized optical microscopy (POM) measurements (Figure 4). It was clear from this that the material has

Table 1. Transition Temperatures (°C), Enthalpy of Transitions (in kJ/mol), Mesophase Range, and Normalized Entropy for I*n*$_x$, upon the Heating Cycle[a]

comp.	X	*T*/°C (Δ*H*/kJ mol^{-1})	Δ*T*	Δ*S*/*R*
I8a	NO_2	Cr 108.1 (47.7) N 189.0 (1.9)	80.9	0.49
I8b	F	Cr 111.4 (43.2) N 144.8 (2.1)	33.4	0.60
I8c	Cl	Cr 97.6 (41.4) N 187.4 (1.8)	89.8	0.47
I8d	OCH_3	Cr 120.0 (53.8) N 245.0 (1.7)	125.0	0.39
I8e	$N(CH_3)_2$	Cr 127.5 (41.6) N 200.9 (1.4)	73.4	0.36
I12a	NO_2	Cr 104.5 (41.6) N 171.2 (2.4)	66.7	0.65
I12b	F	Cr 103.2(39.7) SmA 167.4 (3.3)	64.2	0.90
I12c	Cl	Cr 101.3 (37.8) N 178.1 (2.2)	76.8	0.59
I12d	OCH_3	Cr 110.0 (51.5) N 232.9 (2.0)	122.9	0.48
I12e	$N(CH_3)_2$	Cr 135.8 (49.0) SmA 220.7(1.9)N 228.7 (1.2)	92.9	0.29

[a]Cr, crystal; N, nematic; SmA, smectic A; *T*, temperature; Δ*H*, enthalpy; Δ*T*, mesomorphic range; Δ*S*/*R*, normalized entropy.

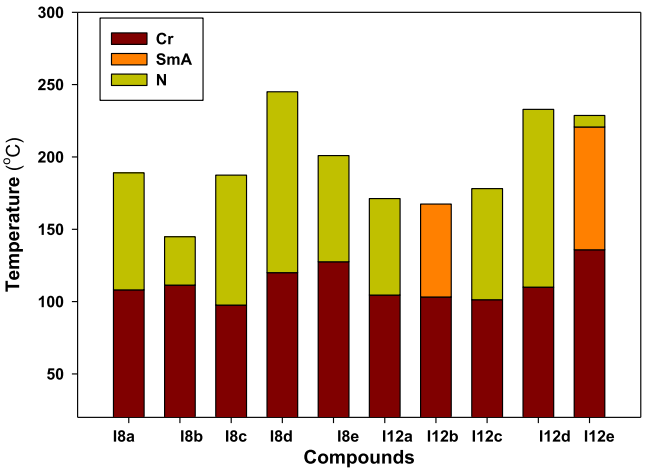

Figure 2. Mesomorphic behavior of the prepared materials **I***n*$_x$ as observed after the second heating rate.

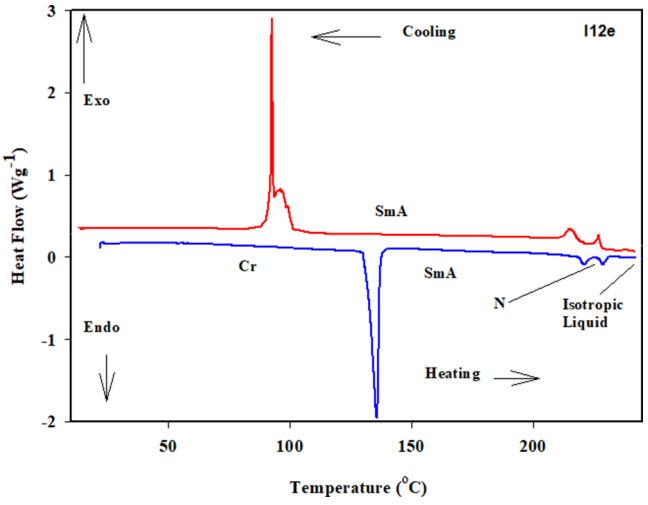

Figure 3. DSC thermograms of **I12**$_e$: recorded from second heating and cooling scans at a rate of 10 °C/min.

enantiotropic monomorphic properties. To evaluate how the length of the terminal alkoxy chain impacts their behavior in the mesophase, Figure 2 graphically represents the transition temperatures of all of the derivatives that have been evaluated.

https://doi.org/10.1021/acsomega.4c01564
ACS Omega 2024, 9, 31601−31610

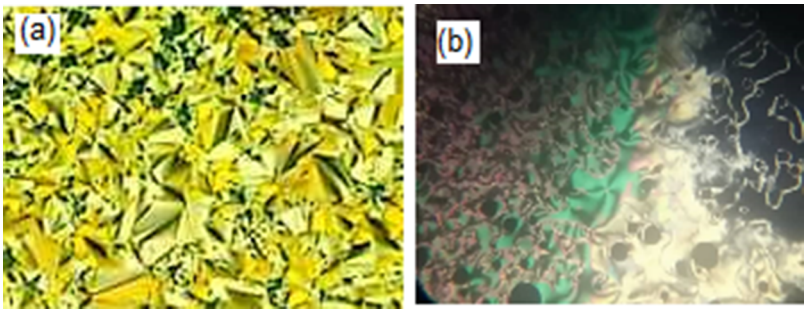

Figure 4. POM textures during heating of compound **I12$_e$**: (a) SmA phase at 180 °C and (b) N phase at 224 °C.

The melting transitions (Cr/SmA) of the studied derivatives display a different pattern as the alkoxy chain length is increased from n = 8 to 12, as can be seen in Table 1 and Figure 2. The melting point typically rises with the increased polarizability of derivatives within the same series. However, the observed trend did not conform to this common rule. However, such a tendency is not consistent with this overarching rule as reported in our previous work.[40−44] Additionally, each homologue of the homologous series is found to be enantiotropic and possesses excellent thermal stability in the mesophase, with a broad temperature mesomorphic range. Thus, for electron-withdrawing terminal NO_2-substituted homologues (**In_a**), their molecules are monomorphic exhibiting only the enantiotropic N phase. Their N temperature ranges ($\Delta T = T_N - T_{Cr}$) decreased from 80.9 to 66.7 °C with increasing alkoxy chain length from n = 8 to n = 12. Compounds with terminal F-substituent (**In_b**) are also found to be monomorphic possessing purely nematogenic mesophase for the short terminal chain length (n = 8) and show the smectogenic phase (SmA phase) for n = 12. Its thermal stability increases from 144.8 to 167.4 °C with increasing n from 8 to 12 as well as ΔT is enhanced from 33.4 to 64.2 °C as n increases from 8 to 12. For X= Cl (**In_c**), all homologues exhibit only the N phase, irrespective of alkoxy chain length, with relatively high thermal stability compared with those of **In_b**. ΔT is reduced from 89.8 to 76.8 °C. The Cl-substituted analogues possess the highest mesomorphic temperature ranges for electron-withdrawing substituted derivatives. Compounds with electron-donating group CH_3O (**In_d**) possess an N mesophase, with high thermal stability and a broad range. ΔT is slightly decreased from 125.0 to 122.9 °C with increasing n from 8 to 12 carbons. **N(CH$_3$)$_2$** substituted derivatives (**In_e**) were shown to exhibit the N phase for n = 8 and are dimorphic possessing both the SmA and N mesophases for n = 12 with high thermal stabilities. The stability of the nematic phase diminishes for all series, regardless of the polarity of substituent X, while the SmA phase increases as normal with the lengthening of the terminal alkoxy chain.[45,46] The downward trend in the thermal transition of the nematic (N) phase is due to the dilution of the rigid mesogenic core. However, as the length of the alkoxy chains increases, the smectic A (SmA) phase appears, decreasing the temperature range of the nematic phase. This likely occurs because increasing the length of the terminal alkyl chain widely promotes microphase separation and facilitates the lamellar structure required for the formation of the smectic phase.[47]

Based on the results mentioned earlier, the thermal stability of the formed mesophase for n = 8 declines in the following order: $CH_3O > N(CH_3)_2 > NO_2 > Cl > F$, while for n = 12, it decreases in the order: $CH_3O > N(CH_3)_2 > Cl > NO_2 > F$. Their mesomorphic range ΔT is found to decrease in the following order: $CH_3O > Cl > NO_2 > N(CH_3)_2 > F$ for n = 8, while for n = 12, the mesophase temperature range decreases in the following order: $CH_3O > N(CH_3)_2 > Cl > NO_2 > F$.

Several factors are usually cited as critical in determining the stability of mesophases and their textures, including the polarity of substituent groups, polarizability, aspect ratio, stiffness, and molecular structure. These factors influence the mesophase behavior to varying degrees. It is generally understood that the stability of a mesophase in a given mesomorphic compound improves with enhanced polarity or polarizability in the mesogenic core, which is typically driven by the polarity of substituent groups, thereby affecting the polarity of the entire molecule.

For the present series of compounds, the estimated entropy change of the mesophase transitions ($\Delta S/R$) is shown in Table 1. An uneven trend and modest magnitudes of $\Delta S/R$ are seen, independent of the length of the molecules as a function of the terminal alkoxy chain. Changes in molecular interactions between molecules may be responsible for the variance and complexity in the entropy change with compact terminal group X and alkoxy chain length. Although the lengthening of the alkoxy chain reduces the strength of core−core contacts, it raises the polarizability of the entire molecule, which strengthens the forces of intermolecular adhesion between neighboring molecules and enhances the degree of molecular ordering. The removal of the lengthy orientational order and the rise in the number of conformational distributions during the mesophase transitions are likely to be blamed for the increase in $\Delta S/R$ values with increasing number of carbons in the alkoxy chain. Higher $\Delta S/R$ magnitude, especially when associated with SmA−isotropic transition as in the case of **I12$_b$** derivatives, is the result of terminally substituting with a polarizable F atom. This process causes the dipole moment of molecules to increase, which improves the lateral interaction and subsequently allows the molecules to pack more efficiently in the liquid crystal phase. Furthermore, the effect of shape and specifically the biaxiality of the molecule play important roles in the entropy change results. The greater the biaxiality, the smaller the orientational order of the nematic phase, and this reduces the N−I entropy changes as reported in previous research studies.[48]

2.2. DFT Theoretical Studies. Quantum chemical calculations provide a powerful tool for understanding the behavior and properties of liquid crystals and are essential for developing new materials with improved performance characteristics. Optimized molecular structures of the synthesized compounds **I12$_{a-e}$** are presented in Figure 5. The thermodynamic parameters as well as the energetics are listed as examples in Table 2.

Generally, the molecular structures of liquid crystals are typically characterized by a high degree of planarity, meaning that the molecules largely lie flat and are oriented in specific

https://doi.org/10.1021/acsomega.4c01564
ACS Omega 2024, 9, 31601−31610

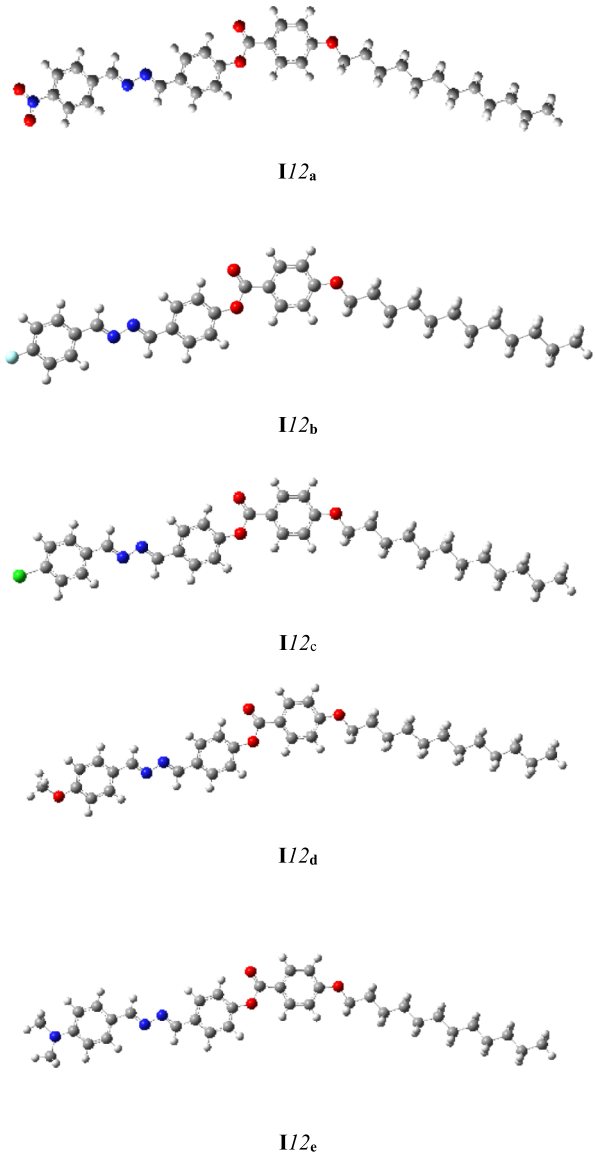

Figure 5. Optimized geometries of series $I12_x$ at the B3LYP/6-31+G(d,p) level of theory.

directions relative to each other. This planarity is essential for the specific alignment of the liquid crystal molecules and consequently for the creation of the ordered phases that are characteristic of such materials. The degree of planarity varies depending on the specific type of liquid crystal molecules and accordingly is influenced by factors such as the molecular structure and temperature and external influences such as electric or magnetic fields. Overall, the high degree of planarity in liquid crystals plays a critical role in their unique properties and makes them useful in a wide range of applications, including in displays, sensors, and optical devices.

As illustrated in Figure 5, all molecular configurations are almost planar, as per the terminal aryl ring that bearing the dodecyloxy group possesses a dihedral angle of ≈0.1°, concerning the central ring. On the other side, the other terminal ring has been proven to lie in the same plane as the central ring; thus, both rings form a dihedral angle of ≈0.1−0.2° concerning the molecular plane of the bis-Schiff base central linking group. Such an extremely small value of the dihedral angle indicates that the entire molecule deviates barely from planarity. Furthermore, the results indicated that the molecular geometry and molecular planarity are not significantly affected by changing the polar X group from an electron-withdrawing group (NO_2, F, and Cl) to an electron-donating group (OMe and NMe_2). As a result, molecular packing in the condensed liquid crystalline phase is enhanced and improved, depending on the molecular planarity of the investigated compounds $\mathbf{I}_{a-e}$. Even though our results offer a reliable estimate of the necessary molecular structure in the gas phase, it should be noted that the presence of these compounds in the condensed liquid crystalline phases might show some variations.

Dipole moment and polarizability are important factors of liquid crystals that allow them to be used in a variety of applications and affect their behavior in electric and magnetic fields. The dipole moment is a measure of the polarity of the molecules, which determines the orientational order of the liquid crystal.[49] The dipole moment enables the external electric field to influence the liquid crystal's alignment, resulting in the formation of distinctive features in the material, such as LCDs and photonic crystal fibers. Moreover, the polarity and interactions between adjacent liquid crystal molecules influence the mesophase temperature range, which affects the stability of the liquid crystal.[50] Polarizability, on the other hand, refers to the ability of a material to be deformed by an electric field. Liquid crystals have high polarizability, which means that they can be easily distorted by an external electric field. This property is important in the electro-optical response of liquid crystals, where the alignment of the molecules can be changed by applying an electric field. Furthermore, the polarizability of the molecule contributes to the magnitude of the intermolecular interactions and provides stability to the structure, and stability leads to durability and enhanced functionality. The density functional theory (DFT)-calculated dipole moments and molecule polarizability for the titled compounds $I12_{a-e}$ at the same level of theory are displayed in Table 3. The results showed that changing the terminal X group from an electron-donating group (OMe and NMe_2) to an electron-attracting group (Cl, F, and NO_2) increases the molecular polarity, ranging from 2.619 to 10.727 D.

The results revealed that the molecule with an electron-donating methoxy-substituted compound, $I12_d$, is less polar than the other compounds in the series $I12_{a-e}$. However, the highest value of the dipole moment was observed for the electron-donating nitro-substituted molecule, $I12_a$. On the other

Table 2. Energy and Thermodynamical Properties of the Optimized Structures (in Hartree) for $I12_{a-e}$

	E_0	E_{298}	H_{298}	G_{298}	S (cal/mol-kelvin)
I12a	−1820.522458	−1820.481448	−1820.480504	−1820.608539	269.473
I12b	−1715.298659	−1715.259409	−1715.258465	−1715.380935	257.759
I12c	−2075.657559	−2075.617863	−2075.616919	−2075.741194	261.558
I12d	−1730.526692	−1730.485687	−1730.484743	−1730.610732	265.165
I12e	−1749.930912	−1749.888167	−1749.887223	−1750.017333	273.840

https://doi.org/10.1021/acsomega.4c01564
ACS Omega 2024, 9, 31601−31610

Table 3. Quantum Chemical Characteristics for the Optimal Structures of the Investigated Molecules, $I12_{a-e}$[a]

E (a.u)	I12a	I12b	I12c	I12d	I12e
dipole moment (D)	10.727	6.394	6.910	2.619	3.991
polarizability (α)	512.54	471.969	490.685	501.426	539.989
E_{HOMO} (eV)	−6.533	−6.227	−6.274	−5.841	−5.225
E_{LUMO} (eV)	−3.334	−2.303	−2.385	−2.055	−1.871
ΔE (eV)	3.199	3.924	3.889	3.786	3.354
IP (eV)	6.533	6.227	6.274	5.841	5.225
EA (eV)	3.334	2.303	2.385	2.055	1.871
μ (eV)	−4.934	−4.265	−4.330	−3.948	−3.548
χ (eV)	4.934	4.265	4.330	3.948	3.548
η (eV)	1.599	1.962	1.944	1.893	1.677
σ (eV^{-1})	0.625	0.510	0.514	0.528	0.596
S (eV^{-1})	0.313	0.981	0.972	0.946	0.838
ω (eV)	7.609	4.636	4.821	4.117	3.754
ΔN_{max}	3.085	2.174	2.227	2.086	2.116

[a] E_{HOMO}: energy of the highest occupied molecular orbital; E_{LUMO}: energy of the lowest unoccupied molecular orbital; ΔE: energy gap between the HOMO and LUMO; IP: ionization potential; EA: electron affinity; χ: absolute electronegativity; μ: chemical potentials; η: absolute hardness; σ: absolute softness; ω: global electrophilicity; S: global softness; and ΔN_{max}: additional electronic charge.

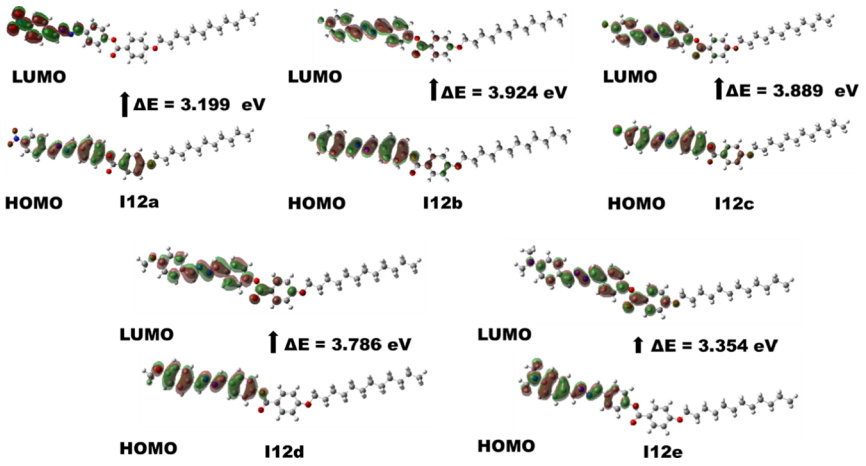

Figure 6. FMOs for the prepared series $I12_{a-e}$ were calculated at the B3LYP/6-31+G(d,p) level of theory.

hand, polarizability has different values according to terminal group X. Compound $I12_e$ is more polarizable than the other compounds (see Table 3). We can conclude that the dipole moment and polarizability with different extents affect the stability of the resulting liquid crystal phase. The presence of nematic and smectic phases for compound $I12_e$ could be explained in terms of the increment of polarizability.

Quantum chemical parameters are vital for the study of liquid crystals.[49,51,52] These parameters help us to predict the stability of the molecule, understand molecular interactions, estimate the optical properties, and design new liquid crystal materials. One of the most important quantum chemical parameters in the study of liquid crystals is the energy of the highest occupied molecular orbital (HOMO) and the lowest unoccupied molecular orbital (LUMO). These parameters help to predict the stability of liquid crystals.[53] Additionally, the absorption and emission spectra of liquid crystals are influenced by their molecular structure and electronic transitions. The HOMO−LUMO energy gap (ΔE) can be used to predict the electronic transitions that occur in the UV−vis region of the spectrum.[54] The DFT calculations of investigated compounds $I12_{a-e}$ revealed that the energy values of HOMO or LUMO are affected by the X group of the terminal ring. Accordingly, the X group has an impact on the HOMO−LUMO energy gap (ΔE), which varies between 3.199 and 3.924 eV and follows the order I12b > $I12_c$ > $I12_d$ > $I12_e$ > $I12_a$. Additionally, the relatively modest energy gaps for all of the compounds under investigation show how soft and reactive these molecules are. The HOMO and LUMO electron densities are primarily confined over the central ring, methineazo-azomethine linker, and the terminal ring containing the X group, as shown in Figure 6. Moreover, the terminal dodecyloxy chain does not participate in the HOMO or LUMO electron densities. Furthermore, absolute electronegativity, χ, chemical potentials, μ, absolute hardness, η, absolute softness, σ, global electrophilicity, ω, global softness, S, and additional electronic charge, ΔN_{max}, which provide clues regarding the reactivity and stability of the molecules under study, have been determined using the HOMO and LUMO energies (Table 3). These properties are critical for the development of innovative liquid crystal technologies because they influence the materials' stability, reactivity, and susceptibility to external fields.

The study of molecular electrostatic potential (MEP) is an important component of liquid crystal research, providing valuable information about the chemical and physical properties of these materials and enabling the design of new liquid crystal materials with improved properties. MEP is a measure of the

https://doi.org/10.1021/acsomega.4c01564
ACS Omega 2024, 9, 31601−31610

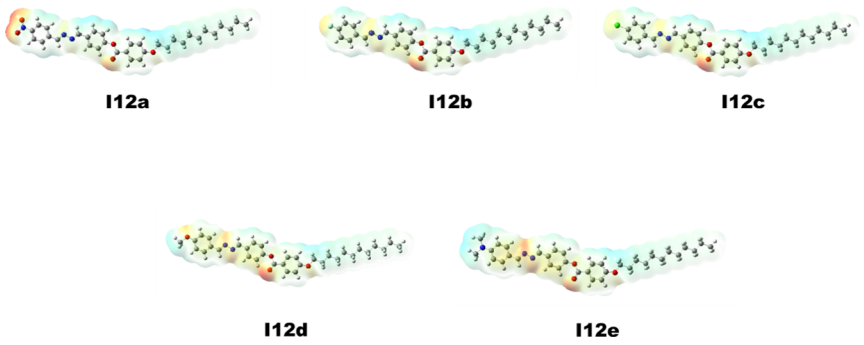

Figure 7. MEPs of the homologous series $I12_{a-e}$.

electric potential energy that exists around a molecule and is determined by the distribution of its electrons.[55]

One of the key properties of liquid crystals is their ability to align themselves in a particular direction in response to an external electric field. This property, known as an electro-optical response, is critical for the operation of LCDs used in televisions, smartphones, and other electronic devices. MEP plays a crucial role in understanding the electro-optical properties of liquid crystals.[56] By modeling the MEP of liquid crystal molecules, researchers can predict how these molecules will behave in an electric field and design new liquid crystal materials with improved properties. Furthermore, MEP is also important for understanding the behavior of liquid crystals in solution.[13] The interaction between liquid crystal molecules and solvents can affect their stability, solubility, and other physical properties. By measuring the MEP of the solvents, researchers can determine which solvents are most compatible with certain liquid crystal molecules and optimize the formulation of liquid crystal solutions. MEP of compounds $\mathbf{I12_{a-e}}$ has been calculated using geometries of compounds optimized at B3LYP/6-31+G(d,p). The MEP's negative sites, which appear red, have a larger electron density and are more reactive as nucleophiles. Positive sites (green or blue) are electrophilic sites and have a low electron density. The potential energy range of our potential map is found to be −5.407e−2 to +5.407e−2 esu. In all the $\mathbf{I12_{a-e}}$ series, as shown in Figure 7, the carbonyl oxygen of the ester linking group and oxygen of the nitro group represent the nucleophilic centers with high electron density, while low electron density is observed near the dodecyl chain. The configuration of the linked alkoxy chain influences the orientation of the charge distribution map, which can impact the type of mesophase through changes in the competitive interactions between end-to-end and side-by-side interactions. The correlation between theoretical charge distribution and observed mesophase types has been reported.[44,57,58]

To study how the size of the terminal substituent influences the mesophase behavior of synthesized compounds, we examined the relationship between the nematic−isotropic transition temperature (T_{N-I}) and the van der Waals radius of the terminal substituent, X. This relationship is depicted for compounds $\mathbf{I8_{a-e}}$ in Figure 8. It was evident that the transition temperatures do not follow a linear correlation with the shape of the terminal substituent regardless of the length of the alkoxy chain. Compounds with electron-withdrawing moieties (F, NO_2, and Cl) and terminal substituents displayed lower nematic−isotropic transition temperatures (T_{N-I}) compared to their corresponding terminal electron−donating groups (OCH_3 and $N(CH_3)_2$). This indicates that the shape of the terminal substituent influences the mesophase behavior,

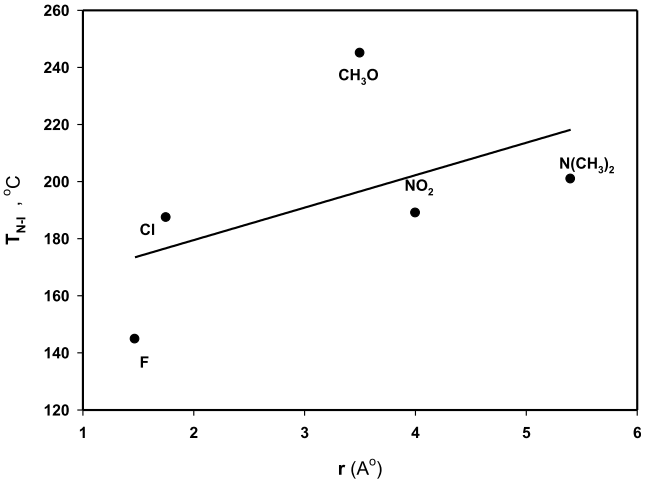

Figure 8. Relationship between the nematic−isotropic transition temperature and the van der Waals radius of the terminal substituent, X, for compounds $\mathbf{I8_{a-e}}$.

although the relationship is more or less linearly dependent on the size of the terminal substituent.[59,60]

3. EXPERIMENTAL SECTION

3.1. Materials. 4-Hydroxybenzaldehyde, 4-nitrobenzaldehyde, 4-fluorobenzaldehyde, 4-chlorobenzaldehyde, 4-anisaldehyde, 4-(dimethylamino)benzaldehyde, hydrazine hydrate, 4-octoyloxybenzoic acid, and 4-dodecyloxybenzoic acid were purchased from Sigma-Aldrich (Germany). Dichloromethane, *N,N′*- dicyclohexylcarbodiimide (DCC), ethanol, and 4-dimethylaminopyridine (DMAP) were purchased from Aldrich (Wisconsin, USA).

3.2. Synthesis. The mesomorphic derivatives $\mathbf{I}n_{a-e}$ were synthesized as detailed in Scheme 1.

3.2.1. Synthesis of 4-((E)-((E)-(4-Substitutedbenzylidene)-hydrazono)methyl)phenol.

A. To a stirred hot ethanolic solution of hydrazine hydrate (10.1 mmol, 15 mL), an ethanolic solution of 4-hydroxybenzaldehyde (10 mmol, 10 mL) was added dropwise for 15 min. The reaction was completed after heating under reflux for a further 60 min, and the precipitates of the desired product were obtained, which were filtered. Moreover, these were utilized in the next step without further purification.
B. An ethanolic solution of 4-substitutedbenzaldehyde (10 mmol, 10 mL) was added dropwise for 20 min to a stirred ethanolic solution of the product from step A (10.1 mmol,

https://doi.org/10.1021/acsomega.4c01564
ACS Omega 2024, 9, 31601−31610

Scheme 1. Synthesis of 4-Substituted Phenyl Methineazo-Azomethine Phenyl 4-Alkoxybenzoates, In_{a-e}

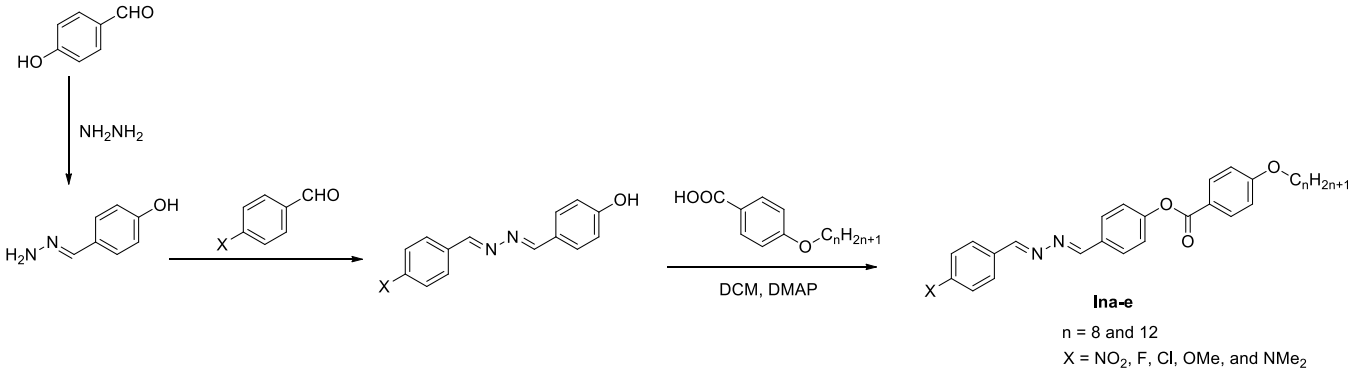

12 mL). After 90 min of continued heating under reflux, the reaction was finished. The precipitates of the products In_{a-e} were obtained, and then filtered, washed, and dried. The product was crystallized from hot ethanol.

3.2.2. Synthesis of 4-((E)-((E)-(4-Substitutedbenzylidene)-hydrazono)methyl)phenyl 4-Alkoxybenzoate, In_{a-e}. Molar equivalents of 4-((*E*)-((*E*)-(4-substitutedbenzylidene)-hydrazono)methyl)phenol and 4-alkoxybenzoic acid (0.01 mol) were dissolved in 25 mL of dry dichloromethane. DCC (0.02 mol) and a few crystals of DMAP, as catalysts, were added. The solution was left to stand for 70 h at room temperature with continuous stirring. The byproduct, dicyclohexylurea, separated was then filtered off, and the filtrate was then evaporated. The obtained solid residue was recrystallized twice from ethanol to give TLC pure products. Full characterization data are given in the Supporting Information (Figures S1−S21).

3.2.2.1. 4-((E)-((E)-(4-Fluorobenzylidene)hydrazono)-methyl)phenol. ^{1}H NMR (400 MHz, DMSO) two isomeric mixtures δ 10.20 (brs, 1H, OH), 10.13 (brs, 1H, OH), 8.72 (d, *J* = 1.9 Hz, 1H, CH═N), 8.68 (d, *J* = 1.5 Hz, 1H, CH═N), 8.61 (s, 1H, CH═N), 8.56 (s, 1H, CH═N), 8.03−7.86 (m, 4H, Ar−H), 7.78−7.67 (m, 4H, Ar−H), 7.35 (q, *J* = 8.2 Hz, 4H, Ar−H), 6.89 (d, *J* = 7.4 Hz, 4H, Ar−H).^{13}C NMR (101 MHz, DMSO) δ 165.63 (C), 165.44 (C), 163.15 (CH), 162.96 (C), 162.20 (C), 161.05 (C), 160.93 (CH), 160.72 (C), 159.78 (CH), 131.24 (CH), 131.15 (CH), 131.10 (C), 130.97 (CH), 130.89 (CH), 130.80 (C), 130.60 (CH), 125.53 (C), 125.22 (C), 116.67 (CH), 116.59 (CH), 116.45 (CH), 116.37 (CH), 116.30 (CH), 116.24 (CH). $C_{14}H_{11}FN_2O$ requires: C, 69.41; H, 4.58; N, 11.56; % found C, 69.23; H, 4.66; N, 11.74%.

3.2.2.2. 4-((E)-((E)-(4-Chlorobenzylidene)hydrazono)-methyl)phenol. ^{1}H NMR (400 MHz, DMSO, D_2O) δ 8.67−8.53 (4s, 2H, CH═N), 7.91−7.80 (m, 2H, Ar−H), 7.70 (dd, *J* = 12.9, 8.7 Hz, 2H, Ar−H), 7.55 (t, *J* = 7.9 Hz, 2H, Ar−H), 6.93−6.83 (m, 2H, Ar−H). $C_{14}H_{11}ClN_2O$ requires: C, 65.00; H, 4.29; Cl, 13.70; N, 10.83; % found: C, 64.80; H, 4.49; N, 10.87%.

3.2.2.3. 4-((E)-((E)-(4-Methoxybenzylidene)hydrazono)-methyl)phenol. ^{1}H NMR (400 MHz, DMSO) two isomeric mixture δ 10.12 (s, 1H, OH), 8.65−8.59 (3s, 4H, CH═N), 7.87−7.79 (m, 4H, Ar−H), 7.72 (d, *J* = 8.6 Hz, 2H, Ar−H), 7.08−7.04 (m, 4H, Ar−H), 6.89−6.87 (m, 2H, Ar−H), 3.84 (s, 6H, 2OCH_3). ^{13}C NMR (101 MHz, DMSO) δ 162.16 (C), 162.07 (C), 161.28 (CH), 160.98 (CH), 160.84 (C), 160.58 (CH), 130.67 (CH), 130.48 (CH), 130.39 (CH), 127.11 (C), 127.02 (C), 125.49 (C), 116.25 (CH), 114.88 (CH), 114.86 (CH), 55.85 (OCH_3), 55.84(OCH_3) $C_{15}H_{14}N_2O_2$ requires: C, 70.85; H, 5.55; N, 11.02; % found: C, 70.75; H, 5.43; N, 11.22%.

3.2.2.4. 4-((E)-((E)-(4-(Dimethylamino)benzylidene)-hydrazono)methyl)phenol. ^{1}H NMR (400 MHz, DMSO) δ 10.06 (s, 1H, OH), 8.55−8.51 (3s, 2H, CH═N), 7.70−7.64 (m, 4H, Ar−H), 6.87 (d, *J* = 8.6 Hz, 2H, Ar−H), 6.78 (d, *J* = 7.9 Hz, 2H, Ar−H), 3.00 (2s, 6H, N(CH_3)$_2$). ^{13}C NMR (101 MHz, DMSO) δ 161.21 (CH), 160.53 (C), 159.88 (CH), 152.48 (C), 130.37 (CH), 130.16 (CH), 125.85 (C), 121.69 (C), 116.20 (CH), 112.15 (CH), 40.19 (CH_3). $C_{16}H_{17}N_3O$ requires: C, 71.89; H, 6.41; N, 15.72; % found: C, 71.67; H, 6.33; N, 15.87%.

3.2.2.5. 4-((E)-((E)-(4-Fluorobenzylidene)hydrazono)-methyl)phenyl 4-(Dodecyloxy)benzoate. ^{1}H NMR (400 MHz, $CDCl_3$) δ 8.66−8.60 (m, 2H, CH═N), 8.13 (dd, *J* = 8.8, 1.9 Hz, 2H, Ar−H), 7.89 (dd, *J* = 8.5, 1.9 Hz, 2H, Ar−H), 7.86−7.80 (m, 2H, Ar−H), 7.32−7.28 (m, 2H, Ar−H), 7.12 (t, *J* = 7.9 Hz, 2H, Ar−H), 6.96 (dd, *J* = 8.7, 1.9 Hz, 2H, Ar−H), 4.03 (t, *J* = 5.3 Hz, 2H, OCH_2), 1.90 (m, 4H, 2CH_2), 1.73 (m, 4H, 2CH_2), 1.55 (m, Hz, 2H, CH_2), 1.43−1.11 (m, 10H, 5CH_2), 0.87 (t, *J* = 6.2 Hz, 3H, CH_3). ^{13}C NMR (101 MHz, $CDCl_3$) δ 165.56 (d, $^1J_{C,F}$ = 253.5 Hz, *C*F), 164.52 (C═O), 163.70 (C), 160.92 (d, $^2J_{C,F}$ = 28.5 Hz, *C*H),, 153.39 (C), 149.63 (CH), 139.77 (C), 132.32 (CH), 131.52 (C), 130.51 (d, $^3J_{C,F}$ = 8.7 Hz, *C*H), 130.37 (C), 129.72 (CH), 122.29 (C), 115.95 (d, $^2J_{C,F}$ = 21.9 Hz, *C*H), 114.34 (CH), 68.33 (OCH_2), 34.90 (CH_2), 31.90 (CH_2), 29.64 (CH_2), 29.54 (CH_2), 29.33 (CH_2), 29.07 (CH_2), 25.96 (CH_2), 25.44 (CH_2), 24.66 (CH_2), 22.67 (CH_2), 14.10 (CH_3). $C_{33}H_{39}FN_2O_3$ requires: C, 74.69; H, 7.41; N, 5.28; % found: C, 74.63; H, 7.55; N, 5.39%.

3.2.2.6. 4-((E)-((E)-(4-Nitrobenzylidene)hydrazono)-methyl)phenyl 4-(Dodecyloxy)benzoate. ^{1}H NMR (400 MHz, $CDCl_3$) δ 8.72 (s, 1H, CH═N), 8.70 (s, 1H, CH═N), 8.32 (d, *J* = 8.7 Hz, 2H, Ar−H), 8.16 (d, *J* = 8.8 Hz, 2H, Ar−H), 8.03 (d, *J* = 8.7 Hz, 2H, Ar−H), 7.95 (d, *J* = 8.6 Hz, 2H, Ar−H), 7.35 (d, *J* = 8.5 Hz, 2H, Ar−H), 7.00 (d, *J* = 8.9 Hz, 2H, Ar−H), 4.06 (t, *J* = 6.5 Hz, 2H, OCH_2), 3.21 (m, 2H, CH_2), 1.93−1.32 (m, 18H, 9CH_2), 0.90 (t, *J* = 6.7 Hz, 3H, CH_3). ^{13}C NMR (101 MHz, $CDCl_3$) δ 164.56 (CO), 163.79 (C), 162.68 (CH), 159.39 (CH), 153.84 (C), 149.09 (C), 139.98 (C), 132.39 (CH), 131.09 (C), 130.11 (CH), 129.06 (CH), 124.03 (CH), 122.47 (CH), 121.06 (C), 114.30 (CH), 68.40 (OCH_2), 34.93 (CH_2), 31.93 (CH_2), 29.64 (CH_2), 29.57 (CH_2), 29.36 (CH_2), 29.09 (CH_2), 25.99 (CH_2), 25.46 (CH_2), 24.62 (CH_2), 22.70 (CH_2), 14.13(CH_3). $C_{33}H_{39}N_3O_5$ requires: C, 71.07; H, 7.05; N, 7.53; % found: C, 71.23; H, 7.25; N, 7.53%.

3.2.2.7. 4-((E)-((E)-(4-Methoxybenzylidene)hydrazono)-methyl)phenyl 4-(Octyloxy)benzoate. ^{1}H NMR (400 MHz, $CDCl_3$) δ 8.68 (s, 1H, CH═N), 8.65 (s, 1H, CH═N), 8.17 (d, *J* = 8 Hz, 2H, Ar−H), 7.92 (d, *J* = 8 Hz, 2H, Ar−H), 7.82 (d, *J* = 8 Hz, 2H, Ar−H), 7.32 (d, *J* = 8 Hz, 2H, Ar−H), 6.99 (d, *J* = 8 Hz,

https://doi.org/10.1021/acsomega.4c01564
ACS Omega 2024, 9, 31601−31610

4H, Ar−H), 4.06 (t, 2H, OCH_2), 3.88 (s, 3H, OCH_3), 3.24−320 (m, 1H), 1.95−1.32 (m, 12H, $6CH_2$), 0.92 (t, 3H, CH_3). ^{13}C NMR (101 MHz, $CDCl_3$) δ 164.59 (C), 163.71 (C), 162.19 (C), 161.92 (CH), 160.39 (CH), 153.22 (C), 132.36 (CH), 131.83 (C), 130.31 (CH), 129.63 (CH), 126.82 (C), 122.28 (CH), 121.22 (C), 114.37 (CH), 114.30 (CH), 68.37 (CH_2), 55.35 (CH_2), 34.94 (CH_2), 31.82 (CH_2), 29.23 (CH_2), 26.00 (CH_2), 22.67 (CH_2), 14.12 (CH_3). $C_{30}H_{34}N_2O_4$ requires C, 74.05; H, 7.04; N, 5.76; % found: C, 74.08; H, 7.22; N, 5.87%.

3.2.2.8. 4-((E)-((E)-(4-Methoxybenzylidene)hydrazono)-methyl)phenyl 4-(Dodecyloxy)benzoate. ^1H NMR (400 MHz, $CDCl_3$) δ 8.66 (s, 1H, CH═N), 8.63 (s, 1H, CH═N), 8.15 (d, J = 8.8 Hz, 2H, Ar−H), 7.90 (d, J = 8.6 Hz, 2H, Ar−H), 7.80 (d, J = 8.7 Hz, 2H, Ar−H), 7.30 (d, J = 8.5 Hz, 2H, Ar−H), 6.97 (dd, J = 8.8, 2.1 Hz, 4H, Ar−H), 4.04 (t, J = 6.5 Hz, 2H, OCH_2), 3.87 (s, 3H, OCH_3), 3.26−3.12 (m, 6H, $3CH_2$), 1.99−1.13 (m, 14H, $7CH_2$), 0.89 (t, J = 6.7 Hz, 3H, CH_3). ^{13}C NMR (101 MHz, $CDCl_3$) δ 164.57 (C), 163.69 (C), 162.17 (C), 161.88 (CH), 160.35 (CH), 153.20 (C), 132.33 (CH), 131.82 (C), 130.28 (CH), 129.59 (CH), 126.80 (C), 122.25 (CH), 121.19 (C), 114.34 (CH), 114.27 (CH), 68.21 (CH_2), 55.64 (OCH_3), 34.92 (CH_2), 31.91 (CH_2), 29.65 (CH_2), 29.55 (CH_2), 29.34 (CH_2), 29.08 (CH_2), 25.93 (CH_2), 25.45 (CH_2), 24.68 (CH_2), 22.68 (CH_2), 14.12 (CH_3). $C_{34}H_{42}N_2O_4$ requires: C, 75.25; H, 7.80; N, 5.16; % found: C, 75.43; H, 7.65; N, 5.26%.

3.2.2.9. 4-((E)-((E)-(4-(Dimethylamino)benzylidene)-hydrazono)methyl)phenyl 4-(Octyloxy)benzoate. ^1H NMR (400 MHz, $CDCl_3$) δ 8.72 (s, 1H, CH═N), 8.61 (s, 1H, CH═N), 8.17 (d, J = 8.9 Hz, 2H, Ar−H), 7.91 (d, J = 8.6 Hz, 2H, Ar−H), 7.77 (d, J = 8.5 Hz, 2H, Ar−H), 7.31 (d, J = 8.6 Hz, 2H, Ar−H), 7.00 (d, J = 8.9 Hz, 2H, Ar−H), 6.75 (d, J = 8.9 Hz, 2H, Ar−H), 4.06 (t, J = 6.5 Hz, 2H, OCH_2), 3.08 (s, 6H, $N(CH_3)_2$), 1.89−1.78 (m, 2H, CH_2), 1.55−1.43 (m, 2H, CH_2), 1.34 (m, 8H, $4CH_2$), 0.91 (t, J = 6.8 Hz, 3H, CH_3). ^{13}C NMR (101 MHz, $CDCl_3$) δ 164.80, 163.68, 162.84, 161.21, 160.31, 159.17, 152.55, 132.36, 130.46, 129.80, 129.44, 122.22, 121.26, 114.36, 111.79, 68.37 (OCH_2), 40.19 ($N(CH_3)_2$), 31.93 (CH_2), 29.57 (CH_2), 29.37 (CH_2), 29.10 (CH_2), 25.99 (CH_2), 22.71 (CH_2), 14.15 (CH_3). $C_{31}H_{37}N_3O_3$ requires C, 74.52; H, 7.46; N, 8.41; % found: C, 74.74; H, 7.67; N, 8.55%.

3.2.2.10. 4-((E)-((E)-(4-(Dimethylamino)benzylidene)-hydrazono)methyl)phenyl 4-(Dodecyloxy)benzoate. ^1H NMR (400 MHz, $CDCl_3$) δ 8.65 (s, 1H, CH═N), 8.60 (s, 1H, CH═N), 8.14 (d, J = 8.8 Hz, 2H, Ar−H), 7.88 (d, J = 8.6 Hz, 2H, Ar−H), 7.72 (d, J = 8.8 Hz, 2H, Ar−H), 7.31−7.27 (m, 2H, Ar−H), 6.97 (d, J = 8.9 Hz, 2H, Ar−H), 6.72 (d, J = 8.9 Hz, 2H, Ar−H), 4.04 (t, J = 6.5 Hz, 2H, OCH_2), 3.03 (s, 6H, $N(CH_3)_2$), 1.92−1.12 (m, 20H, $10CH_2$), 0.90 (t, J = 6.7 Hz, 3H, CH_3). ^{13}C NMR (101 MHz, $CDCl_3$) δ 164.52, 163.60, 162.82, 159.04, 152.86, 152.47, 139.75, 132.26, 130.20, 129.32, 122.12, 114.27, 111.59, 77.38, 77.06, 76.74, 68.28 (OCH_2), 40.06 (CH_2), 34.86 ($N(CH_3)_2$), 31.74 (CH_2), 29.27 (CH_2), 29.16 (CH_2), 29.08 (CH_2), 25.93 (CH_2), 25.39 (CH_2), 24.47 (CH_2), 22.60 (CH_2), 14.05 (CH_3). $C_{35}H_{45}N_3O_3$ requires C, 75.64; H, 8.16; N, 7.56; % found: C, 75.33; H, 8.24; N, 7.76%.

4. COMPUTATIONAL METHODS

Computational methods are provided in the Supporting Information.

5. CONCLUSIONS

The effective synthesis of ten new derivatives with bis-Schiff base linking units, ((*E*)-4-((4-(trifluoromethyl)phenyl)diazenyl)-phenyl 4-alkoxybenzoate, provided for experimental and theoretical investigation of both thermal and optical properties. ^1H NMR, ^{13}C NMR, and elemental studies were used to confirm their molecular structures. By using DSC and POM instruments, the mesomorphic and optical activity of produced compounds were examined. The study revealed that all synthesized homologous series exhibit excellent thermal stability over a wide temperature range with different mesomorphic types depending on the attached terminal polar group and the alkoxy chain length. Moreover, the DFT results demonstrated that none of the compounds exhibit twisting moieties in the bis-Schiff base region and are all planar. Finally, the investigated compounds showed correlations between the experimentally determined values of the mesophase data and the projected quantum chemical properties.

■ ASSOCIATED CONTENT

Supporting Information

The Supporting Information is available free of charge at https://pubs.acs.org/doi/10.1021/acsomega.4c01564.

Full characterization information for prepared materials, including ^1H NMR, ^{13}C NMR data, and computational methods (PDF)

■ AUTHOR INFORMATION

Corresponding Authors

Hoda A. Ahmed − *Department of Chemistry, Faculty of Science, Cairo University, Cairo 12613, Egypt;* orcid.org/0000-0003-3966-7024; Email: ahoda@sci.cu.edu.eg

Mohamed A. El-Atawy − *Chemistry Department, Faculty of Science, Alexandria University, Alexandria 21321, Egypt; Chemistry Department, College of Sciences, Taibah University, Yanbu 30799, Saudi Arabia;* orcid.org/0000-0002-5042-5221; Email: mohamed.elatawi@alexu.edu.eg

Authors

Fowzia S. Alamro − *Department of Chemistry, College of Science, Princess Nourah Bint Abdulrahman University, Riyadh 11671, Saudi Arabia*

Nuha Salamah Alharbi − *Chemistry Department, College of Science, Taibah University, Medina 30002, Saudi Arabia*

Nada S. Al-Kadhi − *Department of Chemistry, College of Science, Princess Nourah Bint Abdulrahman University, Riyadh 11671, Saudi Arabia*

Omaima A. Alhaddadd − *Chemistry Department, College of Science, Taibah University, Medina 30002, Saudi Arabia*

Magdi M. Naoum − *Department of Chemistry, Faculty of Science, Cairo University, Cairo 12613, Egypt*

Complete contact information is available at: https://pubs.acs.org/10.1021/acsomega.4c01564

Notes

The authors declare no competing financial interest.

■ ACKNOWLEDGMENTS

The authors extend their sincere appreciation to "Princess Nourah bint Abdulrahman University Researchers Supporting Project number (PNURSP2024R107), Princess Nourah bint Abdulrahman University, Riyadh, Saudi Arabia".

REFERENCES

(1) Kudreyko, A.; Chigrinov, V.; Hegde, G.; Chausov, D. Photo-aligned Liquid Crystalline Structures for Photonic Applications. *Crystals* **2023**, *13* (6), 965.

(2) d'Alessandro, A.; Asquini, R. Light propagation in confined nematic liquid crystals and device applications. *Applied Sciences* **2021**, *11* (18), 8713.

(3) Uchida, J.; Soberats, B.; Gupta, M.; Kato, T. Advanced functional liquid crystals. *Adv. Mater.* **2022**, *34* (23), No. 2109063.

(4) Du, X.; Liu, Y.; Wang, F.; Zhao, D.; Gleeson, H. F.; Luo, D. A fluorescence sensor for Pb2+ detection based on liquid crystals and aggregation-induced emission luminogens. *ACS Appl. Mater. Interfaces* **2021**, *13* (19), 22361−22367.

(5) Prakash, J.; Parveen, A.; Mishra, Y. K.; Kaushik, A. Nanotechnology-assisted liquid crystals-based biosensors: Towards fundamental to advanced applications. *Biosens. Bioelectron.* **2020**, *168*, No. 112562.

(6) Joralmon, D.; Alfarhan, S.; Kim, S.; Tang, T.; Jin, K.; Li, X. Three-dimensional printing of liquid crystals with thermal sensing capability via multimaterial vat photopolymerization. *ACS Applied Polymer Materials* **2022**, *4* (4), 2951−2959.

(7) Abbasi Moud, A. Chiral liquid crystalline properties of cellulose nanocrystals: fundamentals and applications. *ACS omega* **2022**, *7* (35), 30673−30699.

(8) Alamro, F. S.; Ahmed, H. A.; Bedowr, N. S.; Khushaim, M. S.; El-Atawy, M. A. New advanced liquid crystalline materials bearing bis-azomethine as central spacer. *Polymers* **2022**, *14* (6), 1256.

(9) Kovalchuk, A. I.; Kobzar, Y. L.; Tkachenko, I. M.; Kurioz, Y. I.; Tereshchenko, O. G.; Shekera, O. V.; Nazarenko, V. G.; Shevchenko, V. V. Photoactive fluorinated poly (azomethine) s with azo groups in the main chain for optical storage applications and controlling liquid crystal orientation. *ACS Applied Polymer Materials* **2020**, *2* (2), 455−463.

(10) Gomha, S. M.; Ahmed, H. A.; Shaban, M.; Abolibda, T. Z.; Khushaim, M. S.; Alharbi, K. A. Synthesis, optical characterizations and solar energy applications of new Schiff base materials. *Materials* **2021**, *14* (13), 3718.

(11) Jevtovic, V.; Ahmed, H. A.; Khan, M. T.; Al-Zahrani, S. A.; Masood, N.; Jeilani, Y. A. Preparation of Laterally Chloro-Substituted Schiff Base Ester Liquid Crystals: Mesomorphic and Optical Properties. *Crystals* **2023**, *13* (5), 835.

(12) Hagar, M.; Ahmed, H. A.; Alhaddad, O. A. New azobenzene-based natural fatty acid liquid crystals with low melting point: Synthesis, DFT calculations and binary mixtures. *Liq. Cryst.* **2019**, *46* (15), 2223−2234.

(13) Alamro, F. S.; Ahmed, H. A.; El-Atawy, M. A.; Khushaim, M. S.; Bedowr, N. S.; AL Faze, R.; Al Kadhi, N. S. Physical and Thermal Characterizations of Newly Synthesized Liquid Crystals Based on Benzotrifluoride Moiety. *Materials* **2023**, *16* (12), 4304.

(14) Omar, A. Z.; El-Atawy, M. A.; Alsubaie, M. S.; Alazmi, M. L.; Ahmed, H. A.; Hamed, E. A. Synthesis and Computational Investigations of New Thioether/Azomethine Liquid Crystal Derivatives. *Crystals* **2023**, *13* (3), 378.

(15) El-Atawy, M. A.; Omar, A. Z.; Alazmi, M. L.; Alsubaie, M. S.; Hamed, E. A.; Ahmed, H. A. Synthesis and characterization of new imine liquid crystals based on terminal perfluoroalkyl group. *Heliyon* **2023**, *9* (4), No. e14871, DOI: 10.1016/j.heliyon.2023.e14871.

(16) Strachan, G. J.; Harrison, W. T.; Storey, J. M.; Imrie, C. T. Understanding the remarkable difference in liquid crystal behaviour between secondary and tertiary amides: the synthesis and characterisation of new benzanilide-based liquid crystal dimers. *Phys. Chem. Chem. Phys.* **2021**, *23* (22), 12600−12611.

(17) Strachan, G. J.; Zattarin, A.; Storey, J. M.; Imrie, C. T. Tailoring amide N-substitution to direct liquid crystallinity in benzanilide-based dimers. *Journal of molecular liquids* **2023**, *384*, No. 122160.

(18) Thaker, B.; Kanojiya, J. Mesomorphic properties of liquid crystalline compounds with biphenyl moiety containing azo-ester, azo-cinnamate central linkages and different terminal group. *Liq. Cryst.* **2011**, *38* (8), 1035−1055.

(19) Ahmed, H.; Naoum, M.; Saad, G. Effect of alkoxy-chain length proportionation on the mesophase behaviour of terminally di-substituted phenylazo phenyl benzoates. *Liq. Cryst.* **2013**, *40* (7), 914−921.

(20) Ichimura, K. Photoalignment of liquid-crystal systems. *Chem. Rev.* **2000**, *100* (5), 1847−1874.

(21) Ikeda, T. Photomodulation of liquid crystal orientations for photonic applications. *J. Mater. Chem.* **2003**, *13* (9), 2037−2057.

(22) Blatch, A.; Luckhurst, G. The liquid crystal properties of symmetric and non-symmetric dimers based on the azobenzene mesogenic group. *Liq. Cryst.* **2000**, *27* (6), 775−787.

(23) Prasad, V. Liquid crystalline compounds with V-shaped molecular structures: synthesis and characterization of new azo compounds. *Liq. Cryst.* **2001**, *28* (1), 145−150.

(24) Sastry, P.; Pardhasaradhi, P.; Srinivasu, C.; Pisipati, V.; Datta Prasad, P. Synthesis, characterisation and phase transition studies in N-(−4-ethyloxybenzylydene)-4'-alkoxyanilines. *Liq. Cryst.* **2016**, *43* (5), 632−638.

(25) Elgueta, E. Y.; Parra, M. L.; Barberá, J.; Vergara, J. M.; Dahrouch, M.; Díaz, E. W. New polycatenar Schiff bases derived from 1, 3, 4-thiadiazole: synthesis, mesomorphism and luminescence behaviour. *Liq. Cryst.* **2016**, *43* (11), 1649−1658.

(26) Henderson, P. A.; Imrie, C. T. Methylene-linked liquid crystal dimers and the twist-bend nematic phase. *Liq. Cryst.* **2011**, *38* (11−12), 1407−1414.

(27) Yeap, G.-Y.; Ha, S.-T.; Lim, P.-L.; Boey, P.-L.; Mahmood, W. A. K.; Ito, M. M.; Sanehisa, S. Synthesis and mesomorphic properties of Schiff base esters ortho-hydroxy-para-alkyloxybenzylidene-para-substituted anilines. *Mol. Cryst. Liq. Cryst.* **2004**, *423* (1), 73−84.

(28) Takezoe, H.; Takanishi, Y. ent-core liquid crystals: their mysterious and attractive world. *Japanese journal of applied physics* **2006**, *45* (2R), 597.

(29) Hagar, M.; Chaieb, K.; Parveen, S.; Ahmed, H. A.; Alnoman, R. B. N-alkyl 2-pyridone versus O-alkyl 2-pyridol: Ultrasonic synthesis, DFT, docking studies and their antimicrobial evaluation. *J. Mol. Struct.* **2020**, *1199*, No. 126926.

(30) Curtarolo, S.; Hart, G. L.; Nardelli, M. B.; Mingo, N.; Sanvito, S.; Levy, O. The high-throughput highway to computational materials design. *Nature materials* **2013**, *12* (3), 191−201.

(31) Wang, W. Y.; Li, J.; Liu, W.; Liu, Z.-K. Integrated computational materials engineering for advanced materials: A brief review. *Comput. Mater. Sci.* **2019**, *158*, 42−48.

(32) Li, Z.; Zhou, B. Theoretical investigation of nonvolatile electrical control behavior by ferroelectric polarization switching in two-dimensional MnCl 3/CuInP 2 S 6 van der Waals heterostructures. *Journal of Materials Chemistry C* **2020**, *8* (13), 4534−4541.

(33) Brédas, J.-L.; Persson, K.; Seshadri, R. Computational design of functional materials. *ACS Publications* **2017**, *29*, 2399−2401.

(34) Jain, A.; Shin, Y.; Persson, K. A. Computational predictions of energy materials using density functional theory. *Nat. Rev. Mater.* **2016**, *1* (1), 1−13.

(35) Greenaway, R. L.; Jelfs, K. E. Integrating computational and experimental workflows for accelerated organic materials discovery. *Adv. Mater.* **2021**, *33* (11), No. 2004831.

(36) Butler, K. T.; Frost, J. M.; Skelton, J. M.; Svane, K. L.; Walsh, A. Computational materials design of crystalline solids. *Chem. Soc. Rev.* **2016**, *45* (22), 6138−6146.

(37) Wang, L.; Nan, G.; Yang, X.; Peng, Q.; Li, Q.; Shuai, Z. Computational methods for design of organic materials with high charge mobility. *Chem. Soc. Rev.* **2010**, *39* (2), 423−434.

(38) Elliott, J. A. Novel approaches to multiscale modelling in materials science. *International Materials Reviews* **2011**, *56* (4), 207−225.

(39) Yao, N.; Chen, X.; Fu, Z.-H.; Zhang, Q. Applying classical, ab initio, and machine-learning molecular dynamics simulations to the liquid electrolyte for rechargeable batteries. *Chem. Rev.* **2022**, *122* (12), 10970−11021.

https://doi.org/10.1021/acsomega.4c01564
ACS Omega 2024, 9, 31601−31610

(40) Ahmed, H. A.; El-Atawy, M. A. Synthesis, mesomorphic and geometrical approaches of new non-symmetrical system based on central naphthalene moiety. *Liq. Cryst.* **2021**, *48* (14), 1940−1952.
(41) Ahmed, H.; Saad, G. Mesophase behaviour of laterally di-fluoro-substituted four-ring compounds. *Liq. Cryst.* **2015**, *42* (12), 1765−1772.
(42) Ahmed, H. A.; Hagar, M.; Alhaddad, O. A. Phase behavior and DFT calculations of laterally methyl supramolecular hydrogen-bonding complexes. *Crystals* **2019**, *9* (3), 133.
(43) Ahmed, H.; Mansour, E.; Hagar, M. Mesomorphic study and DFT simulation of calamitic Schiff base liquid crystals with electronically different terminal groups and their binary mixtures. *Liq. Cryst.* **2020**, *47* (14−15), 2292−2304.
(44) Ahmed, H.; Naoum, M. Mesophase behaviour of azobenzene-based angular supramolecular hydrogen-bonded liquid crystals. *Liq. Cryst.* **2016**, *43* (2), 222−234.
(45) Imrie, C.; Taylor, L. The preparation and properties of low molar mass liquid crystals possessing lateral alkyl chains. *Liq. Cryst.* **1989**, *6* (1), 1−10.
(46) Imrie, C. T. Non-symmetric liquid crystal dimers: how to make molecules intercalate. *Liq. Cryst.* **2006**, *33* (11−12), 1449−1485.
(47) Date, R.; Imrie, C.; Luckhurst, G.; Seddon, J. Smectogenic dimeric liquid crystals. The preparation and properties of the α, ω-bis (4-n-alkylanilinebenzylidine-4′-oxy) alkanes. *Liq. Cryst.* **1992**, *12* (2), 203−238.
(48) Donaldson, T.; Staesche, H.; Lu, Z.; Henderson, P.; Achard, M.; Imrie, C. Symmetric and non-symmetric chiral liquid crystal dimers. *Liq. Cryst.* **2010**, *37* (8), 1097−1110.
(49) Al-Mutabagani, L. A.; Alshabanah, L. A.; Ahmed, H. A.; El-Atawy, M. A. Synthesis, optical and DFT characterizations of laterally fluorinated phenyl cinnamate liquid crystal non-symmetric system. *Symmetry* **2021**, *13* (7), 1145.
(50) El-Atawy, M. A.; Khan, M. T.; Popoola, S. A.; Khushaim, M. S.; Jaremko, M.; Emwas, A.-H.; Alamro, F. S.; Naoum, M. M.; Ahmed, H. A. First mesomorphic and DFT characterizations for 3-(or 4-) n-alkanoyloxy benzoic acids and their optical applications. *Heliyon* **2023**, *9* (9), No. e19384.
(51) Lemaur, V.; da Silva Filho, D. A.; Coropceanu, V.; Lehmann, M.; Geerts, Y.; Piris, J.; Debije, M. G.; van de Craats, A. M.; Senthilkumar, K.; Siebbeles, L. D. A. Charge transport properties in discotic liquid crystals: a quantum-chemical insight into structure−property relationships. *J. Am. Chem. Soc.* **2004**, *126* (10), 3271−3279.
(52) Abozeed, A. A.; Al-Hossainy, A. F.; Tsutsumi, O.; Younis, O. Experimental and theoretical optical characterization of a relatively simple organic molecule incorporating biphenyl, methacrylate, trimethylsilyl acetylene, and liquid crystal. *Opt. Mater.* **2024**, *151*, No. 115324.
(53) Sharma, D.; Tiwari, G.; Tiwari, S. N. Electronic and electro-optical properties of 5CB and 5CT liquid crystal molecules: A comparative DFT study. *Pramana* **2021**, *95* (2), 71.
(54) Hagar, M.; Ahmed, H.; El-Sayed, T.; Alnoman, R. Mesophase behavior and DFT conformational analysis of new symmetrical diester chalcone liquid crystals. *J. Mol. Liq.* **2019**, *285*, 96−105.
(55) Sharma, D.; Tiwari, S. N. Electronic structure and vibrational spectra of 1OCB liquid crystal: a DFT study. *Emerging Materials Research* **2017**, *6* (2), 322−330.
(56) Selvaraj, P.; Subramani, K.; Srinivasan, B.; Hsu, C.-J.; Huang, C.-Y. Electro-optical effects of organic N-benzyl-2-methyl-4-nitroaniline dispersion in nematic liquid crystals. *Sci. Rep.* **2020**, *10* (1), 14273.
(57) El-Atawy, M. A.; Alhaddad, O. A.; Ahmed, H. A. Experimental and geometrical structure characterizations of new synthesized laterally fluorinated nematogenic system. *Liq. Cryst.* **2021**, *48* (15), 2106−2116.
(58) Koshti, R. R.; Vyas, A.; Patel, K. A.; Patel, H. S.; Patel, M. B.; Patel, H. New Schiff's base cinnamates/benzoates liquid crystals with lateral methyl substitutes: characterisation, mesomorphic behaviour and DFT calculation. *Liq. Cryst.* **2022**, *49* (2), 248−263.
(59) Yeap, G. Y.; Osman, F.; Imrie, C. T. Non-symmetric dimers: effects of varying the mesogenic linking unit and terminal substituent. *Liq. Cryst.* **2015**, *42* (4), 543−554.
(60) Bondi, A. V. van der Waals volumes and radii. *J. Phys. Chem.* **1964**, *68* (3), 441−451.

https://doi.org/10.1021/acsomega.4c01564
ACS Omega 2024, 9, 31601−31610